Applied Ocean Research 111 (2021) 102639

Contents lists available at ScienceDirect

Applied Ocean Research

journal homepage: www.elsevier.com/locate/apor

# Experimental measurements of propulsive factors in following and head waves

Simone Saettone [*,a,b], Bhushan Taskar [a], Sverre Steen [b], Poul Andersen [a]

[a] Technical University of Denmark, Kgs. Lyngby, Denmark
[b] Norwegian University of Science and Technology, Trondheim, Norway

ARTICLE INFO

*Keywords:*
Propulsive coefficients in waves
Thrust deduction in waves
Wake fraction in waves
Self-propulsion experiments
Following waves
Benchmark data

ABSTRACT

The results from resistance measurements in calm water and load-varying self-propulsion tests in calm water and regular head and following waves are presented. The experimental campaign is conducted in the large towing tank at SINTEF Ocean (formerly MARINTEK). The openly accessible hull of the single screw Duisburg Test Case is selected as the test case. The wave added resistance, ship motions RAOs, axial wake fraction, thrust deduction fraction, relative rotative efficiency, hull efficiency, propeller open-water efficiency, propeller efficiency behind ship, and propulsive efficiency are determined.

Regarding the calculation of the thrust deduction fraction, the results of the experiments show the effect of utilizing the bare hull resistance instead of the linearly extrapolated ship resistance at zero propeller thrust. If the former is applied, the thrust deduction fraction will be dependent on the load of the propeller. If the latter is utilized, the thrust deduction fraction will be independent of the propeller loading. As expected, the wave added resistance is lower in following waves than in head waves. The heave and pitch motions are larger in head waves, whereas the surge motion is higher in following waves. The effective wake fraction is affected by both the propeller loading and the ship motions. In the case of the former, the higher the propeller loading, the lower the effective wake fraction. For the latter, a general decrease in effective wake fraction is noticed in head waves compared to calm water. On the contrary, the effective wake fraction is higher in following waves in comparison to calm water. The thrust deduction fraction computed with the extrapolated ship resistance appears to be slightly affected by the ship motions. However, a final conclusion was not drawn because of the large uncertainties in the measurements of this propulsive coefficient. The variation in propeller open-water efficiency is mainly related to the change in propeller loading. The relative rotative efficiency is barely affected by both the propeller loading and the motions of the ship. Except in the case of very large wave amplitudes, the hull efficiency is hardly influenced by the ship motions. The propulsive efficiency is primarily affected by the change in propeller open-water efficiency.

Based on the results of the experimental campaign, overload tests in calm water provide a good estimation of the propulsion efficiency in waves for the selected case vessel.

## 1. Introduction

The Energy Efficiency Design Index (EEDI) was introduced by the International Maritime Organization (IMO) to reduce global carbon dioxide emissions of shipping operations. The EEDI promotes the development of more energy-efficient marine propulsion systems. The EEDI formulation can be interpreted as the ratio between the $CO_2$ production potential of the vessel and its transport work. The lower the main engine power, the lower the actual EEDI index of a ship. The installed power of the main engine relies upon the contracted ship speed. The fulfilment of the contract depends on stipulated requirements, which are typically represented by nearly ideal weather conditions. The wind speed is usually assumed to be lower than Beaufort scale 2, and the wave height is supposed to be less than 0.5 m. Actual environmental effects are taken care of by adding a powering margin (known as sea margin) to the estimation of the speed-power relationship for a newly built vessel. The sea margin is evaluated based on either statistical analysis or experience. As a consequence, the ship propulsion system is optimized for operating conditions it may rarely experience. The installed engine power may result to be too small or too high for the actual operating conditions of the ship. The correct evaluation of the engine power requires the accurate estimation of the ship performance in waves.

The prediction of the ship performance in realistic weather

* Corresponding author.

https://doi.org/10.1016/j.apor.2021.102639
Received 16 October 2020; Received in revised form 23 March 2021; Accepted 23 March 2021
Available online 28 April 2021

**Nomenclature**

| | |
|---|---|
| $A_E/A_O$ | blade area ratio |
| $B_{WL}$ | waterline breadth |
| $c$ | propeller chord length |
| $C_{AW}$ | wave added resistance coefficient |
| $C_B$ | block coefficient |
| $d_h$ | hub diameter |
| $D$ | propeller diameter |
| $F_D$ | tow force |
| $F_{T_P=0}$ | extrapolated resistance at zero thrust |
| $F_r$ | Froude number |
| $g$ | gravitational acceleration |
| $GM-T$ | transverse metacentric height |
| $I_{xx}$ | roll moment of inertia |
| $I_{yy}$ | pitch moment of inertia |
| $I_{zz}$ | yaw moment of inertia |
| $J$ | advance coefficient ($V_S/(n_P D)$) |
| $J_0$ | advance coefficient ($V_A/(n_P D)$) |
| $KG$ | vertical centre of gravity from the keel |
| $L_{PP}$ | length between perpendiculars |
| $r_{xx}$ | radius of gyration with respect to x |
| $r_{yy}$ | radius of gyration with respect to y |
| $r_{zz}$ | radius of gyration with respect to z |
| $R_T$ | bare hull resistance |
| $R_{AW}$ | wave added resistance |
| $R_{TW}$ | total resistance in waves |
| $R_{TC}$ | total resistance in calm water |
| $S$ | hull wetted surface |
| $t$ | thrust deduction fraction |
| $t_F$ | thrust deduction fraction computed with $F_{T_P=0}$ |
| $t_R$ | thrust deduction fraction computed with $R_T$ |
| $t_P$ | propeller blade thickness |
| $T_M$ | draft midship |
| $T_P$ | propeller thrust |
| $Q_P$ | propeller torque |
| $V_A$ | averaged axial flow velocity at the propeller plane ($V_S(1-w_E)$) |
| $V_S$ | ship speed |
| $X_{COG}$ | longitudinal position of the center of gravity |
| $Y_1$ | measured response amplitude |
| $Y_{COG}$ | lateral position of the center of gravity |
| $w_E$ | effective wake fraction |
| $\theta$ | trim angle |
| $\Delta_m$ | displacement mass |
| $H_W$ | wave height |
| $\mu$ | wave encounter angle |
| $\zeta_A$ | wave amplitude |
| $\rho$ | water density |
| $\lambda$ | wavelength |
| $T_0$ | propeller thrust in open water |
| $Q_0$ | propeller torque in open water |
| $\eta_H$ | hull efficiency |
| $\eta_D$ | propulsive efficiency |
| $\eta_0$ | propeller open-water efficiency |
| $\eta_R$ | relative rotative efficiency |
| $\eta_B$ | propeller efficiency behind ship |
| $x_1$ | measured amplitude of the surge motion |
| $x_3$ | measured amplitude of the heave motion |
| $x_5$ | measured amplitude of the pitch motion |
| $P$ | propeller pitch |
| $F_{D_L}$ | linear tow force |
| $n_P$ | propeller speed |
| $P_E$ | effective power |
| $P_T$ | thrust power |
| $K_T^0$ | measured amplitude of $K_T$ |
| $T_e$ | wave encounter period |
| $RAO_{H-S}$ | Response Amplitude Operator for the heave or surge motion |
| $RAO_P$ | Response Amplitude Operator for the pitch motion |
| $Z$ | number of propeller blades |
| $s$ | wave steepness ($k\,\zeta_A$) |
| $k$ | wave number |
| $c_W$ | wave phase velocity |

conditions compels the understanding of how the propulsion factors are affected by the presence of waves (Taskar et al., 2019). However, the axial wake fraction, thrust deduction fraction, relative rotative efficiency, hull efficiency, propeller open-water efficiency, propeller efficiency behind ship, and propulsive efficiency are traditionally estimated in calm water conditions (Saettone et al., 2018). At the same time, open literature provides limited knowledge of how these propulsive coefficients change in realistic operating conditions, especially in following seas.

The evaluation of the propulsion factors in the presence of waves started in the 1960s. Moor and Murdey (1970) performed self-propulsion model-scale experiments in regular head waves. Three ship models (a medium speed cargo liner, a fast cargo liner, and a tanker) were utilized in both full-load and ballast conditions. The results of the experiments exhibited the largest variation of the propulsive coefficients for the critical wavelengths. The time-averaged thrust deduction fraction varied up 30%, and the time-averaged effective wake fraction changed up to 45%. Similarly, Nakamura and Naito (1977) carried out self-propulsion model-scale experiments in waves for a single screw high-speed container ship. The model was run in regular and irregular waves. Head and following seas were reproduced. The open-water efficiency decreased notably in the case of severe ship motions, whereas the relative rotative efficiency was hardly affected by the presence of waves. The time-averaged effective wake fraction decreased with the increase of the wave height. The variation of the time-averaged thrust deduction fraction with the wave height was comparatively small. Restrained model tests in regular head waves and forced pitch oscillation tests in calm water were also performed. Based on the results of these last two experiments, Nakamura and Naito (1977) argued that the decrease in time-averaged wake fraction has to be primarily attributed to the pitch motion of the ship. Faltinsen (1980) qualitatively explained this phenomenon by examining the influence of the wave induced motions on the mean pressure along the ship. It was indicated that the pitching motion generates a drop in mean pressure from the middle of the ship towards the stern. This variation in pressure causes the flow to be sucked more towards the aft-most part of the ship, increasing the flow velocities at the propeller plane. Faltinsen (1980) also discussed how overload tests in calm water conditions might provide useful information on how the thrust deduction fraction varies in waves. Ueno et al. (2013) carried out free running tests using a container ship model in regular and irregular waves. The results of the experiments suggested that the larger the propeller loading, the smaller the time-averaged effective wake fraction. Bhattacharyya and Steen (2014) conducted load-varying self-propulsion model-scale experiments for a single-screw cargo vessel at two Froude numbers in regular head waves. The model was equipped with either a ducted or a conventional propeller. The time-averaged effective wake fraction estimated in the case of the conventional propeller had the most significant reduction for the critical

wavelengths. The relative rotative efficiency was barely affected by the presence of waves. A good linear relationship between the tow force and the propeller thrust was noticed in both calm water and waves. Saettone et al. (2020b) studied the importance of considering environmental effects on the estimation of the propulsion system performance of a ship. A full-scale LNG powered vessel (Tavakoli et al., 2020) was utilized as the case study. The quasi-steady approach described by Saettone et al. (2020a) was applied for the propeller analysis. The investigation revealed that neglecting the variation in effective wake fraction would lead to a poor prediction of the propulsion system performance in the presence of waves. Saettone et al. (2021) numerically studied the influence of the propeller loading on the thrust deduction fraction. The commercial SHIPFLOW package version 6.5.09 (Larsson et al., 2020) was utilized as the numerical tool. The single screw model-scale KVLCC2 tanker was chosen as the case study. The results exhibited a non-linear inverse correlation between the thrust deduction fraction and the propeller loading.

This paper presents results from resistance measurements (with rudder and dummy propeller hub) in calm water and load-varying self-propulsion experiments in calm water and regular head and following waves. The goal of this work is to acquire knowledge of how the propulsive coefficients change in realistic operating conditions. Particular attention is given to the influence of ship motions and propeller loading on the thrust deduction fraction, wake fraction, and propulsive efficiency. The time-series of the experiments are made publicly available for validation of software tools and empirical methods. Experiments are video recorded for future use by researchers.

## 2. Case vessel

The publicly available hull of the single screw Duisburg Test Case (DTC) (Moctar et al., 2012) are selected as the model test case. The DTC is a modern 14000 TEU post-Panamax container ship developed at the Institute of Ship Technology, Ocean Engineering and Transport Systems (ISMT) of the University of Duisburg-Essen (UDE). The model is constructed in scale 1:63.65 at SINTEF Ocean in conjunction with the EU research project SHOPERA (Energy Efficient Safe SHip OPERAtion) (Papanikolaou et al., 2016). The vertical centre of gravity of the model is lowered compared to the design value to increase stability. Table 1 shows the main specifications of the DTC hull. Figure 1 shows the underwater part of the hull in calm water conditions. The model is equipped with the fixed-pitch right-handed P1513 propeller (see Table 2). The DTC design features a twisted rudder with a Costa bulb. The base profile is a NACA0018. The projected area of the moveable part of the full-scale rudder is 95.1 $m^2$.

**Table 1**
Ship main specifications (* measured values).

| Symbol | Full Scale | Model Scale |
|---|---|---|
| $L_{PP}$ | 355.0 m | 5.577 m |
| $B_{WL}$ | 51.0 m | 0.801 m |
| $T_M$ | 14.5 m | 0.228 m |
| $\Delta_m$ | 173467.6 t | 672.90 kg* |
| $\theta$ | 0.0 deg | 0.0 deg |
| $C_B$ | 0.6608 | 0.6608 |
| $S$ | 22162.99 $m^2$ | 5.471 $m^2$ |
| $KG$ | 19.851 m | 0.236 m* |
| $X_{COG}$ | >174.059 m | 2.721 m* |
| $Y_{COG}$ | 0.000 m | 0.000 m* |
| $I_{xx}$ | 7.15E+07 t $m^2$ | 68.40 kg $m^2$* |
| $I_{yy}$ | 1.31E+09 t $m^2$ | 1249.22 kg $m^2$* |
| $I_{zz}$ | 1.33E+09 t $m^2$ | 1268.40 kg $m^2$* |
| $r_{xx}$ | 20.30 m | 0.319 m |
| $r_{yy}$ | 86.755 m | 1.363 m |
| $r_{zz}$ | 87.400 m | 1.373 m |
| $GM - T$ | 5.100 m | 0.156 m* |

**Fig. 1.** Underwater part of the DTC hull in calm water conditions.

**Table 2**
Propeller main characteristics (* measured values).

| Symbol | Full Scale | Model Scale |
|---|---|---|
| $Z$ | 5 | 5 |
| $D$ | 8.911 m | 0.140 m* |
| $P/D_{0.7}$ | 0.959 | 0.959* |
| $A_E/A_O$ | 0.800 | 0.800 |
| $d_h/D$ | 0.176 | 0.176* |
| $c_{0.7}/D$ | 0.3600 | 0.3600* |
| $(t_P/c)_{0.7}$ | 0.0198 | 0.0198* |

## 3. Model-scale tests

### 3.1. Test facility

The experimental campaign is conducted in the large towing tank at SINTEF Ocean. The main dimensions are 260 m length, 10.5 m width, and 10 m depth. The towing tank is equipped with two carriages: one for traditional calm water tests (maximum towing speed 10 m/s) and one for seakeeping tests (maximum towing speed 5 m/s). Regular and irregular waves are generated by a double flap wavemaker placed on one end of the tank. The maximum wave height is 0.9 m, and the range of the wave period is 0.8-5 sec.

### 3.2. Test set-up

Figure 2 shows a schematic of the arrangement implemented for the experimental campaign. The model is connected to the seakeeping carriage by both lightweight wires and a transverse beam installed on the model deck at amidships. Two force transducers, one port side and one starboard, are attached to the beam to measure the tow force. The spring stiffness is set to avoid resonance related issues. Specifically, the eigenfrequency of the model in surge direction is less than $1/8.5^{th}$ of the lowest wave encounter frequency. The wave calibration is performed without the presence of the model to ensure the accuracy of the generated waves. Three fixed probes (two attached to the carriage and one located at approximately 10 m from the wavemaker) are used to monitor the regularity of the waves along the travel path. The six degrees of motions of the model are recorded with the optoelectronic measuring OQUS system. A dynamometer is used to measure the propeller thrust,

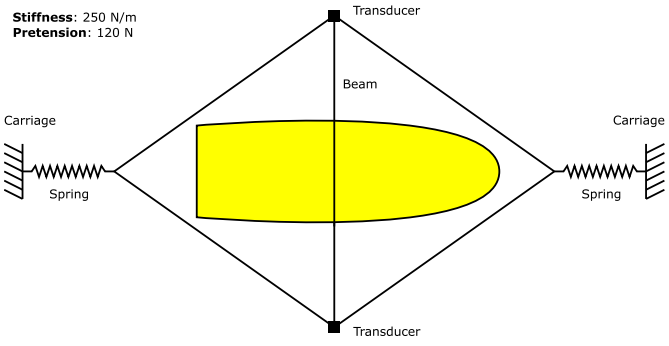


**Fig. 2.** Model-test set-up.

torque and rate of revolutions. Five accelerometers (three at the aft perpendicular, one at amidships, and one at the forward perpendicular) are placed to record the acceleration of the model for quality control of the measured motions. The wave elevation is measured at the forward perpendicular for head waves and at the aft perpendicular in the case of following waves. The wavemaker flap motion is also recorded. The minimum waiting time between consecutive runs is set to 20 minutes to obtain comparable conditions for each of the runs and to produce consistency in the results.

### 3.3. Coordinate system

A right-handed coordinate system with the x-axis positive towards the bow, y-axis pointing starboard, and z-axis positive downwards is applied. The wave direction is relative to the ship: 180° is head waves, whereas 0° is following waves.

### 3.4. Model-test program

Table 3 displays the test conditions carried out in the experiments. In addition to the classic resistance test in calm water (with rudder and dummy propeller hub), load-varying self-propulsion tests in regular head and following waves and calm water are performed. In this type of propulsion experiment, the speed of the model is fixed, and the propeller speed is varied. Traditionally, this procedure is referred to as the British Method for propulsion tests. Table 4 shows the propeller speeds and the velocity of the model implemented in the experiments. The four propeller rates of revolutions are obtained in calm water conditions. The lowest rps represents the close-to-zero thrust. The highest propeller speed represents the close-to-zero tow force. The two additional values are intermediate points. These four propeller speeds are also utilized in the remaining test conditions to consider the influence of the propeller loading and wave-induced ship motions on the propulsive coefficients separately. In a load-varying self-propulsion test the propeller rate of revolutions is generally adjusted several times throughout a run to speed-up the testing process. In the current experimental campaign, only two propeller speeds are implemented each run (run 1: 1.A-1.B and run 2: 2.A-2.B) to achieve adequate precision in the estimation of the propulsive coefficients.

### 3.5. Analysis of the results

The time windows are selected to include a minimum of fifteen wave encounter periods in following waves and twenty-five wave encounter cycles in head waves. A steady-state response is achieved for the time windows utilized in the analysis. A visual inspection of the data is applied to identify the steady-state condition. The unavoidable wave damping causes the wave amplitude to be slightly lower for the run located farther away from the position of the wavemaker. The quadratic relationship between the wave added resistance and the measured wave amplitude is applied as a correction for the tow force to achieve adequate accuracy in the evaluation of the propulsive coefficients. The lowest propeller speed (5 rps) is not included in the analysis of the results, but it is only utilized to confirm the linear relationship between the tow force $F_D$ and the propeller thrust $T_P$ at low propeller loadings. This is because the zero thrust condition is too far from the realistic operating conditions of the ship.

**Table 3**
Test cases overview.

| ID | $\lambda/L_{PP}$ [−] | $H_W$ [m] | $\mu$ [deg] | $s$ [−] | $c_W$ [m/s] |
|---|---|---|---|---|---|
| $R_0$ | Resistance in calm water with rudder and dummy propeller hub | | | | |
| $C_0$ | Self-propulsion in calm water | | | | |
| $F_{W1}$ | 0.5 | 0.092 | 0.0 | 0.103 | 2.086 |
| $F_{W2}$ | 0.5 | 0.128 | 0.0 | 0.144 | 2.086 |
| $F_{W3}$ | 1.0 | 0.084 | 0.0 | 0.048 | 2.950 |
| $F_{W4}$ | 1.0 | 0.138 | 0.0 | 0.078 | 2.950 |
| $F_{W5}$ | 1.0 | 0.214 | 0.0 | 0.121 | 2.950 |
| $F_{W6}$ | 2.5 | 0.076 | 0.0 | 0.017 | 4.665 |
| $F_{W7}$ | 2.5 | 0.124 | 0.0 | 0.028 | 4.665 |
| $F_{W8}$ | 2.5 | 0.192 | 0.0 | 0.043 | 4.665 |
| $H_{W1}$ | 0.5 | 0.092 | 180.0 | 0.103 | 2.086 |
| $H_{W2}$ | 0.5 | 0.128 | 180.0 | 0.144 | 2.086 |
| $H_{W3}$ | 1.0 | 0.084 | 180.0 | 0.048 | 2.950 |
| $H_{W4}$ | 2.5 | 0.076 | 180.0 | 0.017 | 4.665 |
| $H_{W5}$ | 2.5 | 0.124 | 180.0 | 0.028 | 4.665 |
| $H_{W6}$ | 2.5 | 0.192 | 180.0 | 0.043 | 4.665 |

**Table 4**
Velocity of the vessel and propeller speeds.

| Run | $n_P$ [rps] | $V_S$ [m/s] | $F_r$ [−] |
|---|---|---|---|
| 1.A | 5 | 1.000 | 0.1352 |
| 1.B | 8 | 1.000 | 0.1352 |
| 2.A | 10 | 1.000 | 0.1352 |
| 2.B | 12 | 1.000 | 0.1352 |

## 4. Estimation of propulsion factors, wave added resistance, and ship motions RAOs

### 4.1. Thrust deduction fraction

The presence of the propeller causes a disparity between the propeller thrust $T_P$ and the bare hull resistance $R_T$. The reduced pressure field over the wetted surface of the hull is the primary reason for this difference. The thrust deduction fraction is generally utilized to quantify this effect.

The results of load-varying self-propulsion tests, in the range of moderate and lightly loaded propellers, normally report an excellent linear relationship between the tow force $F_D$ and the propeller thrust. As a consequence, the best-fit straight line between $F_D$ and $T_P$ is usually utilized to determine the tow force $F_{D_L}$ applied in the computation of the thrust deduction fraction. In the current work, the least-squares method (Luenberger, 1969) is implemented to compute the linear $F_D - T_P$ trend line. In load-varying self-propulsion tests, the ship resistance is generally estimated by linear extrapolation of the $F_D - T_P$ relationship at zero propeller thrust. The extrapolated ship resistance is referred to as $F_{T_P=0}$. The common range of $F_{T_P=0}/R_T$ is $1.01 - 1.04$ (Holtrop, 2001). Figure 3 provides an example of $F_D$, $F_{T_P=0}$, $F_{D_L}$, and $R_T$.

It is necessary to stress the consequences of using $F_{T_P=0}$ in the calculation of the thrust deduction fraction. In the present work, the thrust deduction fraction computed with $F_{T_P=0}$ is referred to as $t_F$ (see

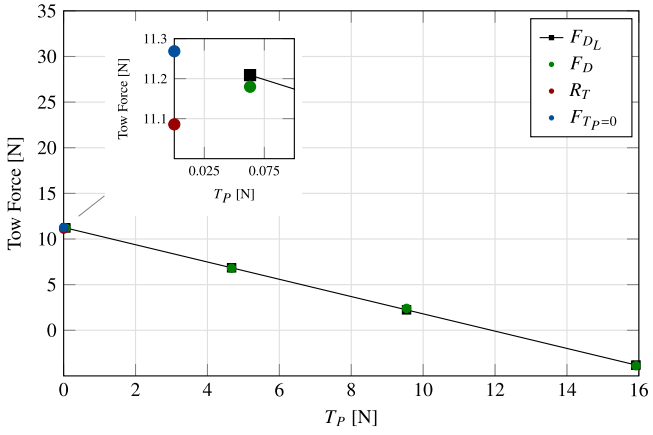


**Fig. 3.** Key points for the evaluation of $t_F$ and $t_R$.

Equation 1), whereas the thrust deduction fraction calculated from $R_T$ is presented as $t_R$ (see Equation 2).

$$t_F = \frac{T_P + F_{D_L} - F_{T_{P=0}}}{T_P} = 1 - \frac{F_{T_{P=0}} - F_{D_L}}{T_P} \tag{1}$$

$$t_R = \frac{T_P + F_{D_L} - R_T}{T_P} = 1 - \frac{R_T - F_{D_L}}{T_P} \tag{2}$$

If the linear relationship between $F_D$ and $T_P$ were applied to compute the ship resistance, the thrust deduction fraction would be independent of the propeller loading. On the contrary, if the thrust deduction fraction were computed with $R_T$, it would be dependent on the load of the propeller. In addition, $t_F$ will always be smaller than $t_R$ if $F_{T_{P=0}}/R_T$ is larger than 1.

Based on these considerations, in the current work, the thrust deduction fraction is computed with both approaches in calm water conditions. This is necessary to show the difference between $t_F$ and $t_R$. In the presence of waves, the thrust deduction fraction is computed with $F_{T_{P=0}}$.

### 4.2. Effective wake fraction

The flow field of a propeller operating behind a ship differs considerably from the open-water condition. The averaged axial flow velocity at the propeller plane $V_A$ is smaller than the speed of the ship $V_S$. The effective wake fraction $w_E$ is commonly utilized to quantify this effect:

$$w_E = 1 - \frac{V_A}{V_S} \tag{3}$$

In the present work, the thrust identity method is applied to determine $w_E$. In this approach, the propeller is assumed to generate the same thrust in a flow field of wake fraction $w_E$ as in the open water condition with speed $V_A$. The advance coefficient obtained from the thrust identity method is generally referred to as $J_0$. Thus, Equation 3 can be rewritten as:

$$w_E = 1 - \frac{J_0}{J} \quad , \quad J = \frac{V_S}{n_P \cdot D} \tag{4}$$

### 4.3. Hull efficiency

The hull efficiency $\eta_H$ represents the influence of the propeller-hull interaction on the efficiency of the propulsion system $\eta_D$. The hull efficiency is defined as the ratio between the effective power $P_E$ and the thrust power $P_T$, and it can be expressed as a function of the effective wake fraction and the thrust deduction fraction. In the current study, the hull efficiency is estimated with $t_F$ ($F_{T_{P=0}}$).

$$\eta_H = \frac{P_E}{P_T} = \frac{R_T \cdot V_S}{T_P \cdot V_A} = \frac{1 - t_F}{1 - w_E} \tag{5}$$

### 4.4. Propeller open-water efficiency

The propeller open-water efficiency $\eta_0$ is defined as the ratio between the thrust power and the power absorbed by the propeller operating in open water conditions. In the present work, the thrust identity method is utilized to determine $Q_0$.

$$\eta_0 = \frac{T_0 \cdot V_A}{2 \cdot \pi \cdot n_P \cdot Q_0} = \frac{T_P \cdot V_A}{2 \cdot \pi \cdot n_P \cdot Q_0} \tag{6}$$

### 4.5. Propeller efficiency behind ship

The propeller efficiency behind ship $\eta_B$ is defined as the ratio between the thrust power and the power absorbed by the propeller operating behind the ship.

$$\eta_B = \frac{T_P \cdot V_A}{2 \cdot \pi \cdot n_P \cdot Q_P} \tag{7}$$

### 4.6. Relative rotative efficiency

The relative rotative efficiency $\eta_R$ is defined as the ratio between the propeller efficiency behind ship $\eta_B$ and the propeller open-water efficiency $\eta_0$.

$$\eta_R = \frac{\eta_B}{\eta_0} = \frac{Q_0}{Q_P} \tag{8}$$

### 4.7. Propulsive efficiency

The propulsive efficiency or quasi-propulsive coefficient $\eta_D$ is the efficiency of the complete propeller-hull hydrodynamic system. It can also be written as the product of the hull efficiency $\eta_H$, propeller open-water efficiency $\eta_0$, and relative rotative efficiency $\eta_R$.

$$\eta_D = \eta_H \cdot \eta_0 \cdot \eta_R \tag{9}$$

### 4.8. Wave added resistance

In energy terms, the wave added resistance $R_{AW}$ is caused by an extra energy loss associated with the encountered wave. It is defined as the difference between the time-averaged total resistance in waves $R_{TW}$ and the resistance in calm water $R_{TC}$. In the current work, $R_{TW}$ and $R_{TC}$ are estimated by linear extrapolation of the $F_D - T_P$ relationship at zero propeller thrust ($F_{T_{P=0}}$). The wave added resistance coefficient $C_{AW}$ is computed as follows:

$$C_{AW} = \frac{R_{TW} - R_{TC}}{\rho g (H_W/2)^2 B_{WL}^2 / L_{PP}} = \frac{R_{AW}}{\rho g (H_W/2)^2 B_{WL}^2 / L_{PP}} \tag{10}$$

### 4.9. Ship motions RAOs

The heave and surge RAOs (Response Amplitude Operators) are defined as the ratio between the measured response amplitude $Y_1$ and the measured wave amplitude $\zeta_A$. For the pitch RAO, the wave number $k$ is added to the denominator.

$$RAO_{H-S} = \frac{Y_1}{\zeta_A} \quad , \quad RAO_P = \frac{Y_1}{s} \tag{11}$$

## 5. Results

### 5.1. Propeller open-water curves

Propeller open-water tests are not performed during the current experimental campaign. Instead, the propeller open-water curves are obtained from previous experiments carried out by SINTEF Ocean for the SHOPERA project. Figure 4 displays the propeller open-water characteristics utilized in the present study.

The time-averaged propeller open-water characteristics in waves are assumed to be equal to the open-water curves in calm water conditions. This assumption is admissible since the propeller is always operating far from the free surface (Faltinsen, 1980).

### 5.2. Tow force vs propeller thrust

Figures 5 and 6 show the time-averaged tow force $F_D$ against the time-averaged propeller thrust $T_P$ in head and following waves. The calm water values are also included for comparison. A good linear correlation between $F_D$ and $T_P$ can be noticed for all the tested cases. This result confirms the linearity between the tow force and the propeller thrust, in both waves and calm water, in the range of moderate and

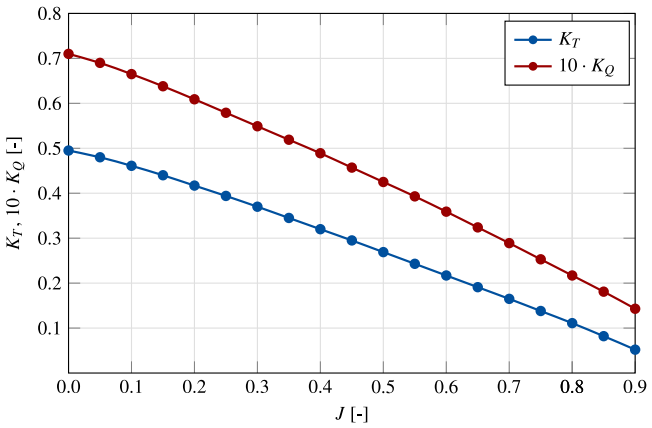


**Fig. 4.** Propeller open-water curves.

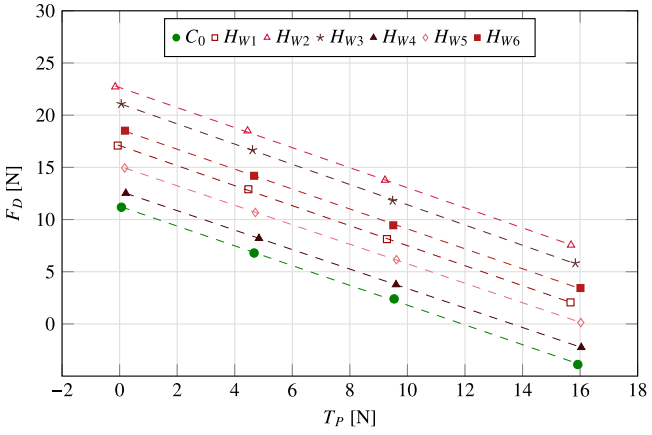


**Fig. 5.** $F_D$ vs $T_P$ with linear trendline in head waves (red) and calm water (green).

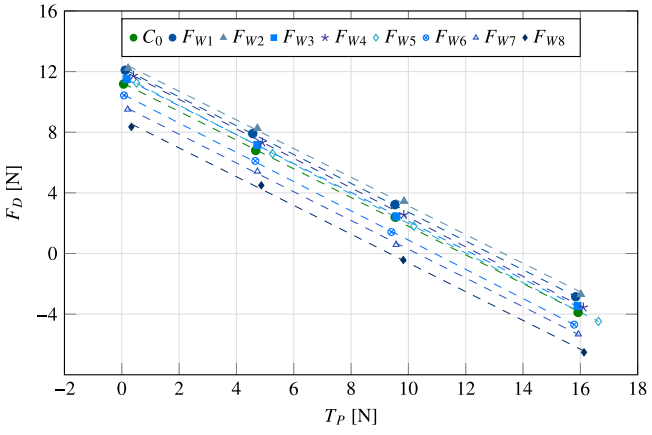


**Fig. 6.** $F_D$ vs $T_P$ with linear trendline in following waves (blue) and calm water (green).

lightly loaded propellers.

The four propeller speeds applied in the experiments are easily identifiable in four clusters of points. For each one of these groups, the propeller thrust is not constant even though the propeller speed is fixed. This is because of the variation in the time-averaged effective wake fraction caused by the presence of the wave.

### 5.3. Wave added resistance

Figure 7 reports the wave added resistance coefficient $C_{AW}$ against the dimensionless wavelength $\lambda/L_{PP}$. Minimal differences can be noticed among the wave added resistance coefficients obtained for the same wavelength and wave direction but different wave height. The estimated added resistance coefficients in head waves are in line with the results obtained by Sprenger et al. (2016) and Lyu and el Moctar (2017). In following waves, $C_{AW}$ is close to zero for $\lambda/L_{PP} = 0.5$ and $\lambda/L_{PP} = 1.0$. At $\lambda/L_{PP} = 2.5$, the ship experiences a pushing effect, leading to a negative $C_{AW}$.

### 5.4. Ship motions RAOs

Figures 8, 9, and 10 show the surge, heave, and pitch RAOs. The motions of the ship are averaged over the range of the three propeller speeds (8, 10, and 12 rps) utilized in the current analysis of the results. Negligible differences can be seen among the RAOs obtained for the same wavelength and wave direction but different wave height. The estimated heave and pitch RAOs in head waves are in line with both the numerical simulations performed by Liu et al. (2014) and the experiments carried out by Lyu and el Moctar (2017). The measured amplitude of the surge motion is higher in following waves than in head waves. A similar trend was reported by Rahaman et al. (2017) and Nakamura and Naito (1977).

### 5.5. Propeller thrust and torque coefficients

Figures 11 and 12 show the time-averaged thrust coefficient $K_T$ and time-averaged torque coefficient $K_Q$ against the dimensionless wavelength $\lambda/L_{PP}$. $K_T$ and $K_Q$ are also averaged over the range of the three propeller speeds (8, 10, and 12 rps) used in the present analysis of the results. In head waves, a general decrease in $K_T$ and $K_Q$ can be noticed compared to calm water. This reduction in $K_T$ and $K_Q$ is related to the mean increase in the axial velocity at the propeller plane. In particular, the thrust and torque coefficients have their minimum at $\lambda/L_{PP} = 0.5$. At $\lambda/L_{PP} = 2.5$, $K_T$ and $K_Q$ tend to their calm water values. In the case of constant wavelength for head waves, the higher the wave amplitude, the lower $K_T$ and $K_Q$. In following waves, a general increase in $K_T$ and $K_Q$ can be observed compared to calm water. This increment is related to the mean increase in effective wake fraction. In the case of constant wavelength for following waves, the larger the wave amplitude, the higher $K_T$ and $K_Q$ are. It is also possible to notice the larger influence of the wave amplitude on $K_T$ and $K_Q$ in following waves than in head waves.

Figure 13 shows the amplitude of the thrust coefficient $K_T^0$ against the dimensionless wavelength $\lambda/L_{PP}$. For the sake of clarity, only six representative cases are presented: $F_{W1}$, $F_{W3}$, $F_{W6}$, $H_{W1}$, $H_{W3}$, and $H_{W4}$. It is

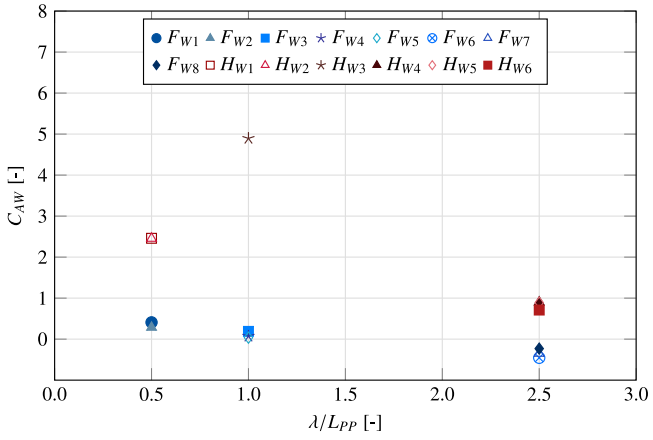


**Fig. 7.** $C_{AW}$ vs $\lambda/L_{PP}$ in following waves (blue) and head waves (red).

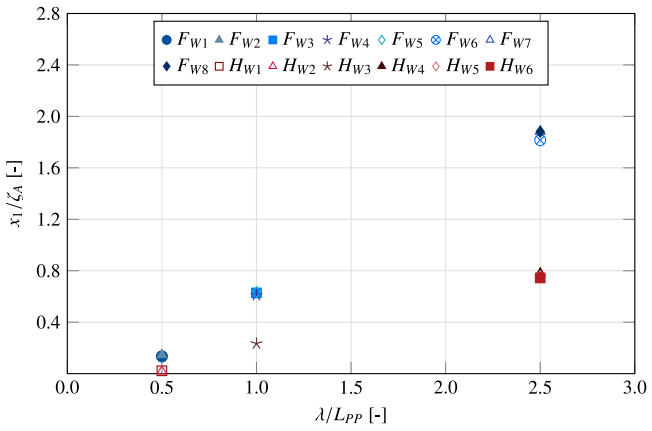


**Fig. 8.** Surge RAO in following waves (blue) and head waves (red).

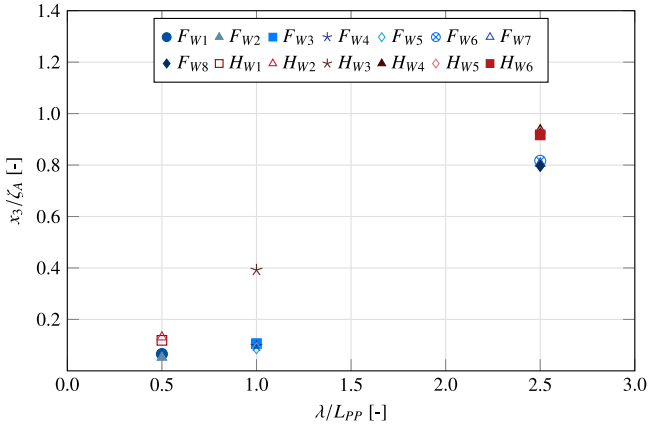


**Fig. 9.** Heave RAO in following waves (blue) and head waves (red).

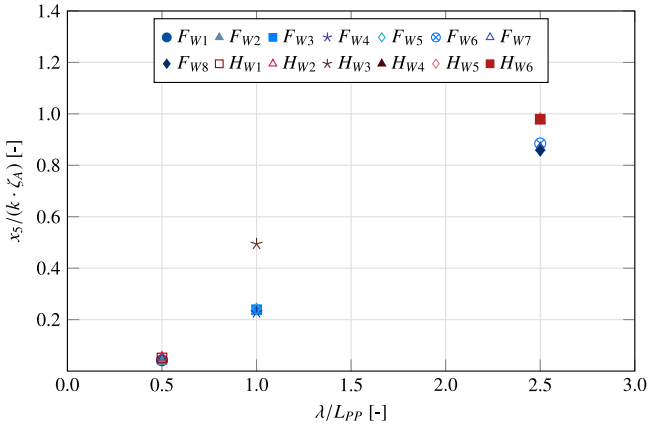


**Fig. 10.** Pitch RAO in following waves (blue) and head waves (red).

possible to notice that the higher the propeller speed, the lower $K_T^0$. This is because the larger the propeller loading, generated by the increased propeller rate of revolutions, the lower the relative variation in the angle of attack caused by the time-varying wake field. At $\lambda/L_{PP} = 2.5$ and $\lambda/L_{PP} = 1.0$, $K_T^0$ is lower in following waves than in head waves. An opposite trend can be seen for $\lambda/L_{PP} = 0.5$.

### 5.6. Bare hull resistance and linearly extrapolated ship resistance

Table 5 shows the bare hull resistance $R_T$ (with rudder and dummy

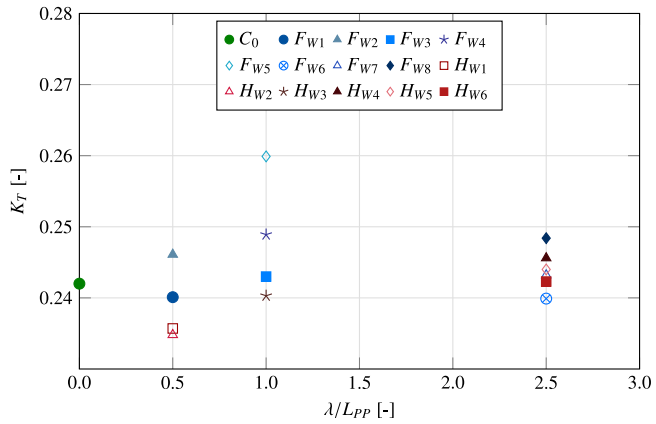


**Fig. 11.** $K_T$ vs $\lambda/L_{PP}$ in following waves (blue), head waves (red), and calm water (green).

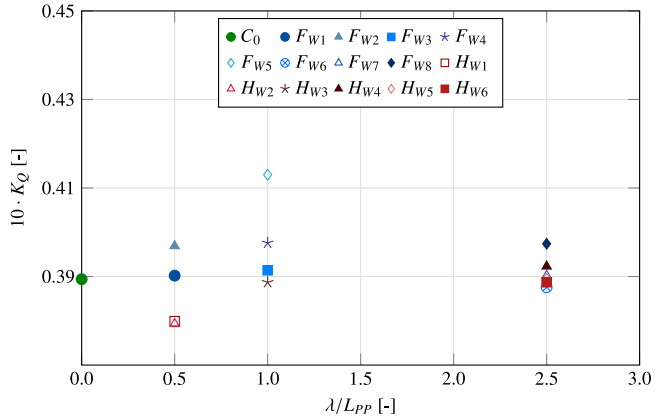


**Fig. 12.** $K_Q$ vs $\lambda/L_{PP}$ in following waves (blue), head waves (red), and calm water (green).

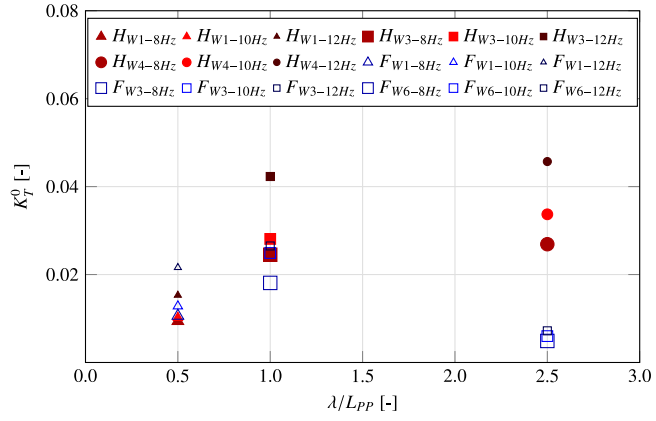


**Fig. 13.** $K_T^0$ vs $\lambda/L_{PP}$ in following waves (blue) and head waves (red).

**Table 5**
Bare hull resistance vs linearly extrapolated ship resistance.

| ID | Resistance [N] |
|---|---|
| $R$ | 11.08 |
| $F_{T_P=0}$ | 11.27 |

propeller hub) and the linearly extrapolated ship resistance $F_{T_P=0}$. The ratio $F_{T_P=0}/R_T$ is equal to 1.017. This confirms the increase in the estimated ship resistance when the $F_D - T_P$ relationship is utilized.

### 5.7. Thrust deduction fraction

Figure 14 shows the time-averaged thrust deduction fractions $t_F$ and $t_R$, computed in calm water conditions, against the propeller thrust $T_P$. It can be noticed the dependency of the propeller loading on $t_R$, and the independency of $t_F$ of the propeller thrust. In addition, $t_R$ results to be greater than $t_F$, and their difference decreases with the increase of the propeller loading. These results prove the importance of utilizing the bare hull resistance in the estimation of the thrust deduction fraction.

Figure 15 displays the time-averaged thrust deduction fraction $t_F$ computed in head and following waves against the dimensionless wavelength $\lambda/L_{PP}$. The calm water values are also included. It is necessary to remind that since $t_F$ is computed, the differences between the thrust deduction fraction in calm water and waves are independent of the propeller loading. Small differences in $t_F$ can be noticed over the range of considered wavelengths. A general decrease in the thrust deduction fraction can be seen compared to calm water. In both head and following waves, the maximum reduction occurs at $\lambda/L_{PP} = 1$.

### 5.8. Effective wake fraction

Figure 16 shows the time-averaged effective wake fraction $w_E$ against the dimensionless wavelength $\lambda/L_{PP}$ in head and following waves. The calm water values are also added for comparison. $w_E$ is also averaged over the range of the three propeller speeds (8, 10, and 12 rps) utilized in the current analysis of the results. Since the thrust identity method is applied to compute $w_E$, the trend of the results resembles the one for $K_T$. A general decrease in $w_E$ can be noticed in head waves compared to calm water. In head waves, the higher the wave amplitude, the lower the effective wake fraction. The minimum values occur at $\lambda/L_{PP} = 0.5$. This indicates that the amplitude of the relative vertical motion at the location of the propeller does not have the largest influence on the effective wake fraction. In following waves, a general increase in $w_E$ can be seen compared to calm water. This might be related to the direct interaction between the propeller and the encountered wave. In following waves, the higher the wave amplitude, the larger the effective wake fraction.

Figure 17 reports the time-averaged effective wake fraction $w_E$ against the time-averaged propeller thrust $T_P$ in head and following waves. In the interests of clarity, only six representative cases are presented: $F_{W5}$, $F_{W6}$, $F_{W7}$, $H_{W1}$, $H_{W2}$, and $H_{W4}$. The calm water values are also included. It can be observed that the higher the propeller loading, the lower the effective wake fraction. This could be the result of the deformation of the boundary layer caused by the increased propeller thrust (Adachi, 1983).

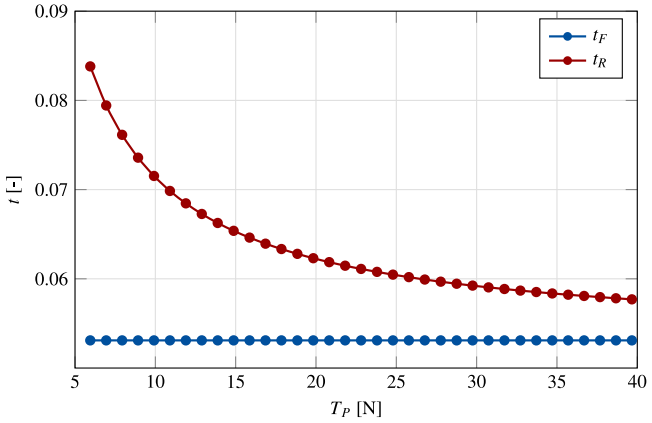


**Fig. 14.** $t_F$ vs $t_R$ in calm water conditions.

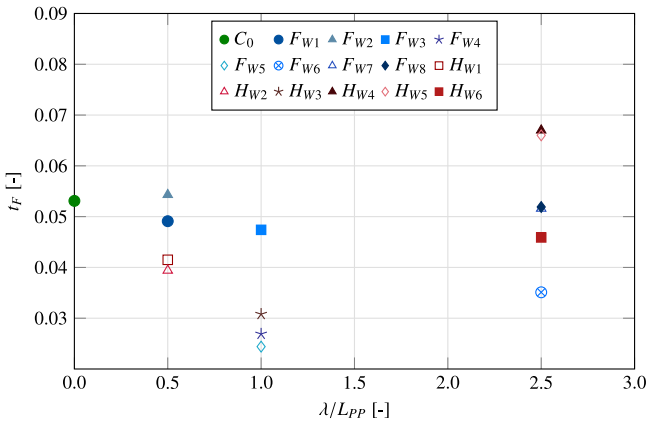


**Fig. 15.** $t_F$ in following waves (blue), head waves (red), and calm water (green).

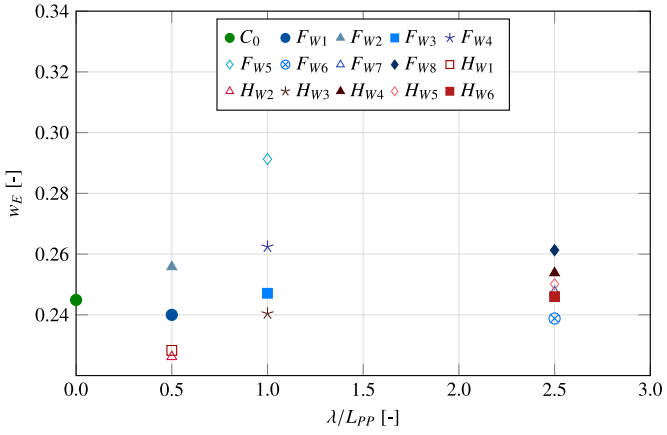


**Fig. 16.** $w_E$ vs $\lambda/L_{PP}$ in following waves (blue), head waves (red), and calm water (green).

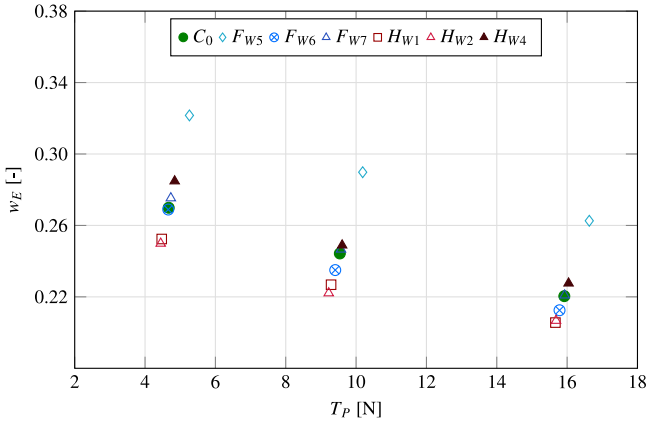


**Fig. 17.** $w_E$ vs $T_P$ in following waves (blue), head waves (red), and calm water (green).

### 5.9. Hull efficiency

Figure 18 shows the time-averaged hull efficiency $\eta_H$ against the dimensionless wavelength $\lambda/L_{PP}$ in head and following waves. The calm water values are also included for comparison. $\eta_H$ is also averaged over the range of the three propeller speeds (8, 10, and 12 rps) used in the analysis of the results. Since the variation in thrust deduction fraction is small, the trend of the results resembles the one for $w_E$. In following

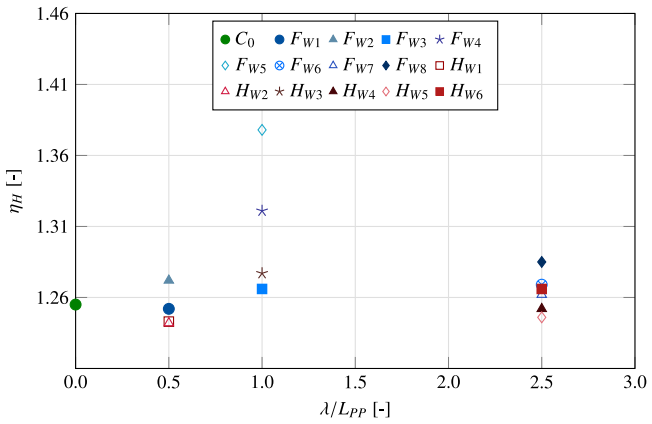


**Fig. 18.** $\eta_H$ vs $\lambda/L_{PP}$ in following waves (blue), head waves (red), and calm water (green).

waves, a general increase in the hull efficiency can be noticed compared to calm water. Except in the case of very large wave amplitudes, small differences in $\eta_H$ can be seen over the range of considered wavelengths. Similar conclusions were drawn by Bhattacharyya and Steen (2014).

Figure 19 displays the time-averaged hull efficiency $\eta_H$ against the time-averaged propeller thrust $T_P$ in head and following waves. The calm water values are also added. In the interests of clarity, only six representative cases are presented: $F_{W5}$, $F_{W6}$, $F_{W7}$, $H_{W2}$, $H_{W4}$, and $H_{W6}$. It can be noticed that the higher the propeller loading, the lower the hull efficiency. A similar trend was reported by Bhattacharyya and Steen (2014).

### 5.10. Relative rotative efficiency

Figure 20 shows the time-averaged relative rotative efficiency $\eta_R$ against the dimensionless wavelength $\lambda/L_{PP}$ in head and following waves. The calm water values are also reported. For the sake of clarity, only six representative cases are presented: $F_{W1}$, $F_{W3}$, $F_{W6}$, $H_{W1}$, $H_{W3}$, and $H_{W4}$. It is possible to observe the negligible influence of both waves and propeller loading on the relative rotative efficiency. Similar results were reported by Moor and Murdey (1970), Nakamura and Naito (1977), Sigmund and el Moctar (2017), and Bhattacharyya and Steen (2014).

### 5.11. Propeller open-water efficiency

Figure 21 shows the time-averaged propeller open-water efficiency $\eta_0$ against the dimensionless wavelength $\lambda/L_{PP}$ in head and following waves. The calm water values are also included. In the interests of clarity, only six representative cases are presented: $F_{W1}$, $F_{W3}$, $F_{W6}$, $H_{W1}$,

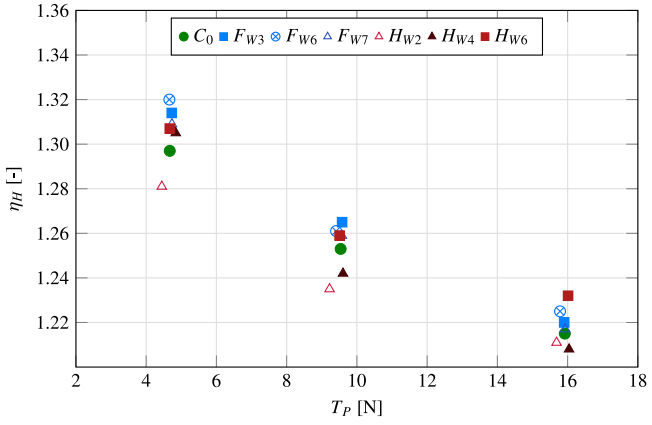


**Fig. 19.** $\eta_H$ vs $T_P$ in following waves (blue) and calm water (green).

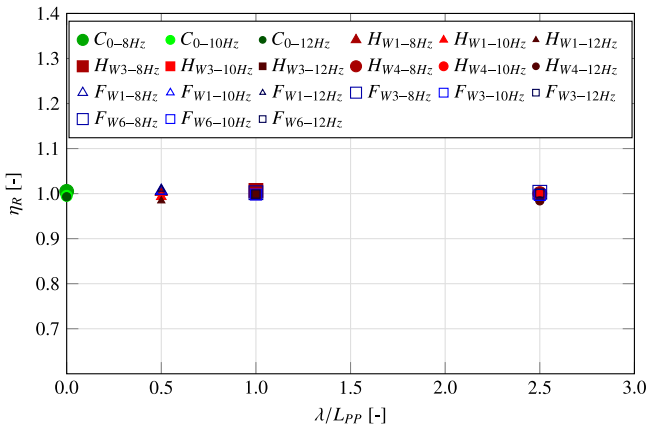


**Fig. 20.** $\eta_R$ vs $\lambda/L_{PP}$ in following waves (blue), head waves (red), and calm water (green).

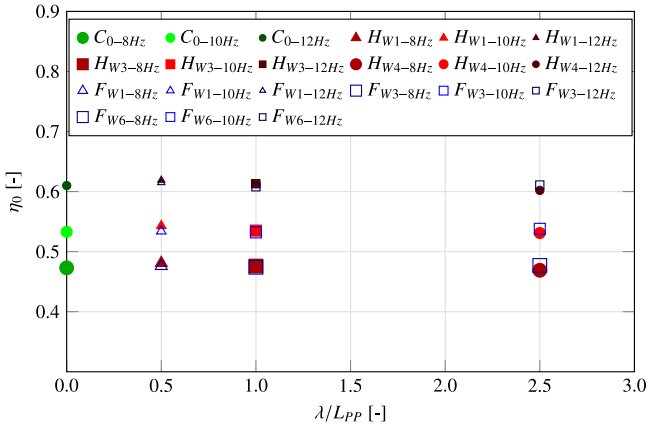


**Fig. 21.** $\eta_0$ vs $\lambda/L_{PP}$ in following waves (blue), head waves (red), and calm water (green).

$H_{W3}$, and $H_{W4}$. The main variation in $\eta_0$ is caused by the change in propeller speed. This is because the propeller loading has a larger influence on the propeller open-water efficiency than the wave-particle velocity and ship motions. As a consequence, the higher the propeller loading, the lower the propeller open-water efficiency. These results indicate that the commonly reported decrease in $\eta_0$ in the range of the critical wavelengths is primarily caused by the large value of wave added resistance.

### 5.12. Propeller efficiency behind ship

Figure 22 shows the time-averaged propeller efficiency behind ship $\eta_B$ against the dimensionless wavelength $\lambda/L_{PP}$ in head and following waves. The calm water values are also added for comparison. For the sake of clarity, only six representative cases are presented: $F_{W1}$, $F_{W3}$, $F_{W6}$, $H_{W1}$, $H_{W3}$, and $H_{W4}$. Since the relative rotative efficiency is influenced by neither the presence of waves nor the propeller loading, the propeller efficiency behind ship resembles the propeller open-water efficiency. Therefore, the same conclusions achieved for $\eta_0$ can be drawn for $\eta_B$.

### 5.13. Propulsive efficiency

Figure 23 shows the time-averaged propulsive efficiency $\eta_D$ against the dimensionless wavelength $\lambda/L_{PP}$ in head and following waves. The calm water values are also added for comparison. In the interests of clarity, only six representative cases are reported: $F_{W1}$, $F_{W3}$, $F_{W6}$, $H_{W1}$, $H_{W3}$, and $H_{W4}$. Compared to $\eta_R$ and $\eta_0$, $\eta_D$ is slightly more affected by the

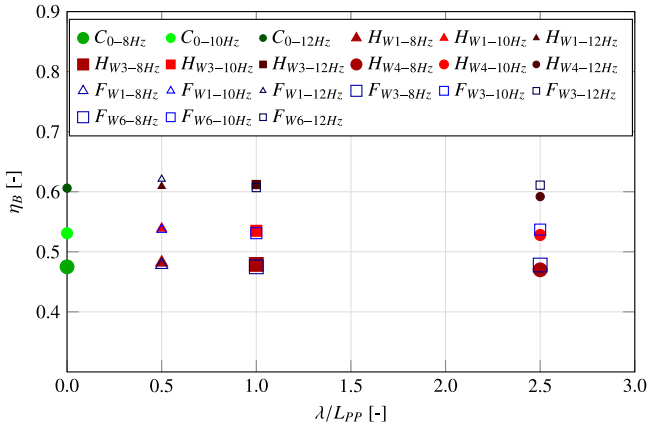


**Fig. 22.** $\eta_B$ vs $\lambda/L_{PP}$ in following waves (blue), head waves (red), and calm water (green).

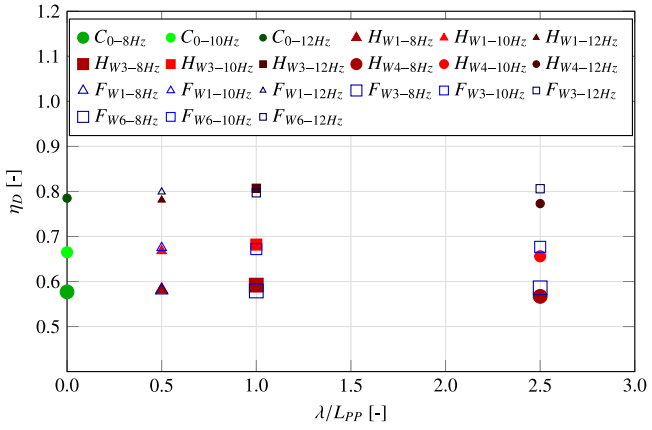


**Fig. 23.** $\eta_D$ vs $\lambda/L_{PP}$ in following waves (blue), head waves (red), and calm water (green).

ship motions. This is because of the small change in $\eta_H$ produced by the encountered waves. However, the main variation in the propulsive efficiency is still caused by the change in propeller loading (variation in $\eta_0$). Therefore, the overload tests carried out in calm water conditions provide a good estimation of the propulsive efficiency in waves. The accuracy of the overload tests in calm water for the evaluation of the propulsive efficiency could be increased by using the exact propulsion point in waves. This would be achieved by utilizing both the effective wake fraction $w_E$ and the thrust deduction fraction $t_F$ determined in the presence of waves.

## 6. Uncertainties

The precision errors $e_s$ and $\bar{e}_s$ (defined in Equation 12) are computed for the propulsive coefficients, propeller speed, ship speed, propeller thrust, thrust coefficient, propeller torque, torque coefficient, extrapolated ship resistance, and tow force.

$$e_s = \frac{t \cdot S_x}{M} \quad , \quad \bar{e}_s = \frac{t \cdot S_x}{\sqrt{N} \cdot M} \tag{12}$$

The two-tailed Student's t-distribution with $N-1$ degrees of freedom is calculated with a cumulative probability of 0.95. Test case $F_{W5}$ is repeated four times to assess the reproducibility and repeatability of the experiments. A minimum of five test cases is run in between the single repeated measurements. Table 6 shows the precision errors achieved for $F_{W5}$. For the sake of completeness, the precision errors $e_s$ and $\bar{e}_s$ are also determined in calm water conditions for the bare hull resistance

**Table 6**
Precision errors $e_s$ and $\bar{e}_s$ for $F_{W5}$.

| Symbol | $e_s$ [%] | $\bar{e}_s$ [%] |
|---|---|---|
| $T_P$ | 0.814 | 0.407 |
| $K_T$ | 0.814 | 0.407 |
| $F_D$ | 2.738 | 1.369 |
| $Q_P$ | 0.279 | 0.139 |
| $K_Q$ | 0.279 | 0.139 |
| $n$ | 0.014 | 0.007 |
| $V_S$ | 0.006 | 0.003 |
| $1-t_F$ | 0.628 | 0.327 |
| $F_{T_P=0}$ | 0.205 | 0.102 |
| $1-w_E$ | 1.077 | 0.538 |
| $\eta_H$ | 0.902 | 0.451 |
| $\eta_B$ | 0.845 | 0.422 |
| $\eta_R$ | 0.713 | 0.357 |
| $\eta_0$ | 0.907 | 0.454 |
| $\eta_D$ | 1.019 | 0.509 |

$R_T$. Test case $R_0$ is repeated four times in between the single repeated measurements. In this case, $e_s$ is 0.873% and $\bar{e}_s$ is 0.437%. These values prove that the presence of the wave increases the uncertainty for the ship resistance, as explained by Park et al. (2015).

Three representative cases are selected to show the measured data's confidence intervals: $K_T$, $w_E$, and $t_F$ in following waves (respectively see Figures 24-25-26). The same uncertainties computed for case $F_{W5}$ are utilized for the confidence intervals of the displayed cases. Regarding the thrust coefficient and effective wake fraction, the measurements are within acceptable limits. Concerning the thrust deduction fraction, it is possible to see several overlaps in the confidence intervals. This outcome is related to two primary reasons. One, the thrust deduction fraction has a very low value for the considered ship. Two, the precision error for the thrust deduction fraction relies upon the simultaneous variation of the propeller thrust, ship resistance, and tow force. A small change in their values enormously impacts the magnitude of this propulsive coefficient. Nevertheless, the conclusions related to thrust deduction fractions $t_R$ and $t_F$ are still valid. This is because their comparison is performed in calm water conditions where the uncertainties are considerably lower than in the presence of waves.

## 7. Conclusions

The results from resistance measurements in calm water and load-varying self-propulsion tests in calm water and regular head and following waves were presented. The linearly extrapolated ship resistance $F_{T_P=0}$ resulted in being 1.7% higher than the bare hull resistance

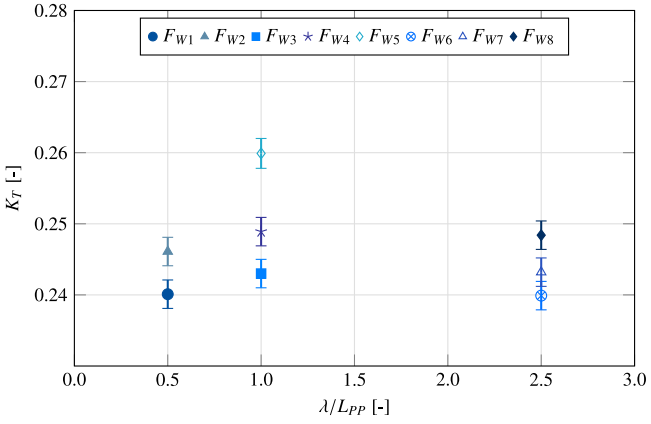


**Fig. 24.** $K_T$ vs $\lambda/L_{PP}$ in following waves with confidence intervals.

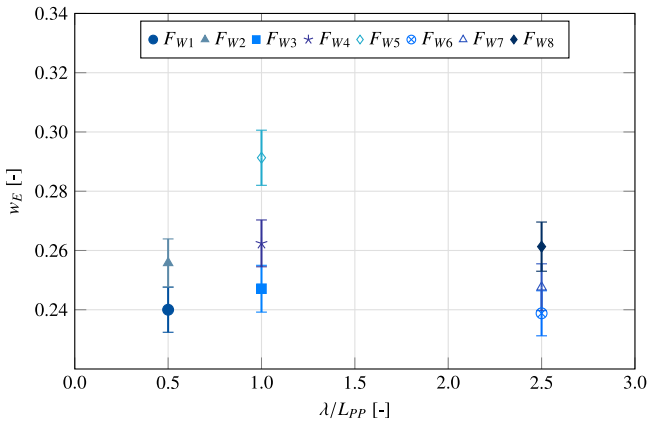


**Fig. 25.** $w_E$ vs $\lambda/L_{PP}$ in following waves with confidence intervals.

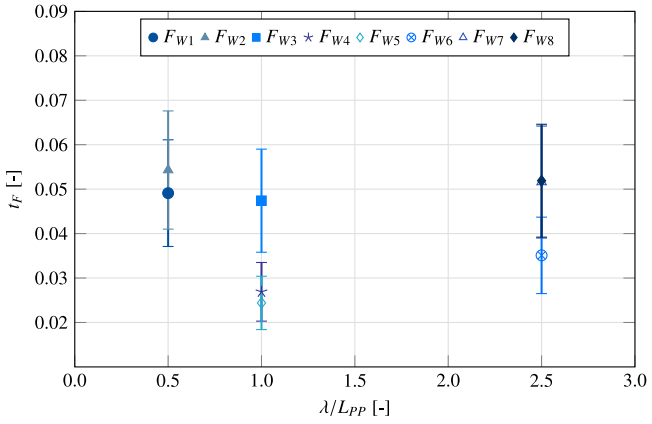


**Fig. 26.** $t_F$ in following waves with confidence intervals.

$R_T$ (with rudder and dummy propeller hub). As a consequence, $t_R$ was greater than $t_F$, and their difference decreased with the increase of the propeller loading. In addition, $t_R$ resulted in being dependent on the propeller loading, whereas $t_F$ was not affected by the variation in the propeller thrust. As expected, the wave added resistance was lower in following seas than in head waves. The pitch and heave and motions were higher in head waves, whereas the surge motion was significantly larger in following waves. The effective wake fraction was affected by both the propeller loading and the ship motions. In the case of the former, the higher the propeller loading, the lower the effective wake fraction. For the latter, a general decrease in effective wake fraction was noticed in head waves compared to calm water. On the contrary, the effective wake fraction was higher in following waves in comparison to calm water. The ship motions appeared to slightly influence the thrust deduction fraction computed with the extrapolated ship resistance. However, since the uncertainties for this propulsive coefficient are quite large, it was difficult to conclude. The change in propeller open-water efficiency was primarily related to the variation in propeller loading. The relative rotative efficiency was hardly influenced by both the propeller loading and the motions of the ship. Except in the case of very large wave amplitudes, the hull efficiency was hardly influenced by the ship motions. The variation in propeller loading mainly influenced the propulsive efficiency. Therefore, overload tests in calm water provided a good estimation of the propulsive efficiency in the range of the considered propeller loadings. However, this conclusion might change for a different ship. This is because the importance of the ship motions and wave-particle velocity in comparison to the propeller loading for the propulsive efficiency depends on several factors, e.g. the magnitude of the wave added resistance and ship motions, ship propulsion point, ship speed, and propeller loading in calm water. As future work, it would be relevant to repeat the same type of experiments for different case vessels.

## CRediT authorship contribution statement

**Simone Saettone:** Conceptualization, Methodology, Software, Validation, Formal analysis, Writing - original draft, Writing - review & editing. **Bhushan Taskar:** Conceptualization, Writing - review & editing. **Sverre Steen:** Conceptualization, Supervision, Project administration, Funding acquisition, Writing - review & editing. **Poul Andersen:** Conceptualization, Supervision, Project administration, Funding acquisition, Writing - review & editing.

## Declaration of Competing Interest

All authors have participated in conception, analysis and interpretation of the data, revising the article critically and approval of the final version. The authors have no affiliation with any organization with a direct or indirect financial interest in the subject matter discussed in the manuscript. The authors confirm that this work is original and has not been published elsewhere.

## Acknowledgements

The model experiments were funded by the Kongsberg Maritime University Technology Centre "Ship Performance and Cyber-Physical Systems" at the Norwegian University of Science and Technology. The authors thank Luca Savio from SINTEF Ocean for helping with the analysis of the results. The authors also express their gratitude to Terje Rosten from the Norwegian University of Science and Technology and Rune Thorbjørnsen from SINTEF Ocean for their support and assistance during the entire experimental campaign.

## Supplementary material

Supplementary material associated with this article can be found at 10.11583/DTU.13090508

## References

Adachi, H., 1983. On the theoretical bases and application methods of the propeller load varying test method. Journal of the Society of Naval Architects of Japan 1983 (154), 109–117.
Bhattacharyya, A., Steen, S., 2014. Propulsive factors in waves: A comparative experimental study for an open and a ducted propeller. Ocean engineering 91, 263–272.
Faltinsen, O.M., 1980. Prediction of resistance and propulsion of a ship in a seaway. Proceedings of the 13th symposium on naval hydrodynamics, Tokyo, 1980.
Holtrop, J., 2001. Extrapolation of propulsion tests for ships with appendages and complex propulsors. Marine Technology 38 (3), 145–157.
Larsson, L., Janson, C. E., Broberg, L., Regnström, B., 2020. SHIPFLOW 6.5 User Manual. FLOWTECH International AB, Gothenburg, Sweden.
Liu, S., Papanikolaou, A., Zaraphonitis, G., 2014. Time Domain Simulation of Nonlinear Ship Motions Using an Impulsive Responsive Function Method. Proceeding of the International Conference on Maritime Technology ICMT, Glasgow, UK, 7th9th July 2014.
Luenberger, D.G., 1969. Optimization by vector space methods. Wiley.
Lyu, W., el Moctar, O., 2017. Numerical and experimental investigations of wave-induced second order hydrodynamic loads. Ocean Engineering 131, 197–212.
Moctar, O.E., Shigunov, V., Zorn, T., 2012. Duisburg Test Case: Post-panamax container ship for benchmarking. Ship Technology Research 59 (3), 50–64.
Moor, D.I., Murdey, D.C., 1970. Motions and Propulsion of Single Screw Models in Head Seas, Part II. Quarterly Transactions of the Royal Institution of Naval Architects 112 (2), 121–127.
Nakamura, S., Naito, S., 1977. Propulsive performance of a container ship in waves. Journal of the Society of Naval Architects of Japan 15.
Papanikolaou, A., Zaraphonitis, G., Bitner-Gregersen, E., Shigunov, V., El Moctar, O., Soares, C.G., Devalapalli, R., Sprenger, F., 2016. Energy efficient safe ship operation (SHOPERA). Transportation Research Procedia 14, 820–829.
Park, D.M., Lee, J., Kim, Y., 2015. Uncertainty analysis for added resistance experiment of KVLCC2 ship, 95, 143–156.

Rahaman, M.M., Islam, H., Akimoto, H., Islam, M.R., 2017. Motion predictions of ships in actual operating conditions using potential flow based solver. Journal of Naval Architecture and Marine Engineering 14 (1), 65–76.

Saettone, S., Taskar, B., Regener, P.B., Andersen, P., 2018. Unsteady propeller forces and hull pressure pulses in waves, Vol. 18, pp. 158–163.

Saettone, S., Taskar, B., Regener, P.B., Steen, S., Andersen, P., 2020. A comparison between fully-unsteady and quasi-steady approach for the prediction of the propeller performance in waves. Applied Ocean Research 99, 102011. https://doi.org/10.1016/j.apor.2019.102011.

Saettone, S., Taskar, B., Steen, S., Andersen, P., 2021. The influence of the propeller loading on the thrust deduction fraction. Ship Technology Research 0 (0), 1–9. https://doi.org/10.1080/09377255.2021.1892934.

Saettone, S., Tavakoli, S., Taskar, B., Jensen, M.V., Pedersen, E., Schramm, J., Steen, S., Andersen, P., 2020. The importance of the engine-propeller model accuracy on the performance prediction of amarine propulsion system in the presence of waves. Applied Ocean Research 103, 102320.

Sigmund, S., el Moctar, O., 2017. Numerical and experimental investigation of propulsion in waves. Ocean Engineering 144, 35–49.

Sprenger, F., Hassani, V., Maron, A., Delefortrie, G., Van Zwijnsvoorde, T., Cura-Hochbaum, A., Lengwinat, A., 2016. Establishment of a validation and benchmark database for the assessment of ship operation in adverse conditions. International Conference on Offshore Mechanics and Arctic Engineering, Vol. 49927. American Society of Mechanical Engineers.V001T01A039

Taskar, B., Regener, P.B., Andersen, P., 2019. The impact of propulsion factors on vessel performance in waves. Sixth International Symposium on Marine Propulsors (smp'19).

Tavakoli, S., Saettone, S., Steen, S., Andersen, P., Schramm, J., Pedersen, E., 2020. Modeling and analysis of performance and emissions of marine lean-burn natural gas engine propulsion in waves. Applied Energy 279, 115904.

Ueno, M., Tsukada, Y., Tanizawa, K., 2013. Estimation and prediction of effective inflow velocity to propeller in waves. Journal of Marine Science and Technology 18 (3), 339–348. https://doi.org/10.1007/s00773-013-0211-8.